# Determination of the beam asymmetry $\Sigma$ in $\eta$- and $\eta'$-photoproduction using Bayesian statistics

Jakob Michael Krause



Masterarbeit in Physik
angefertigt im Helmholtz-Institut für Strahlen- und Kernphysik

vorgelegt der
Mathematisch-Naturwissenschaftlichen Fakultät
der
Rheinischen Friedrich-Wilhelms-Universität
Bonn

Sep 2022

I hereby declare that this thesis was formulated by myself and that no sources or tools other than those cited were used.

Bonn, ................. ...................................
Date Signature

1. Gutachterin: Jun. Prof. Dr. Annika Thiel
2. Gutachter: Prof. Dr. Jochen Dingfelder

# Contents


**1 Introduction** **1**
1.1 Photoproduction of Pseudoscalar Mesons . . . . 4
1.2 Measurement of Polarization Observables . . . . 5
1.3 Introduction to BAYESIAN statistics . . . . 5
1.4 Motivation and Structure of this Thesis . . . . 5

**2 Experimental Setup** **7**
2.1 Production of (polarized) high energy photon beam . . . . 7
2.1.1 Tagger . . . . 8
2.2 Beam Target . . . . 8
2.3 Calorimeters . . . . 8
2.4 Trigger . . . . 8

**3 Event selection** **11**
3.1 Preselection and charge cut . . . . 11
3.2 Time of particles . . . . 12
3.3 Kinematic constraints . . . . 14
3.3.1 Derivation of cut conditions . . . . 14
3.3.2 Determination of cut ranges . . . . 15
3.3.3 Quality of event selection . . . . 21
3.4 Investigation of background and additional cuts . . . . 22
3.4.1 Inspecting plausibility of background reactions . . . . 22
3.4.2 Misidentification of background reactions . . . . 25
3.4.3 Examination of additional cuts . . . . 28

**4 Extraction of the beam asymmetries $\Sigma_\eta$ and $\Sigma_{\eta'}$** **33**
4.1 Methods . . . . 34
4.1.1 Event yield asymmetries . . . . 34
4.1.2 Event based fit . . . . 34
4.2 Determination of $\Sigma_\eta$ using Bayesian statistics . . . . 34
4.2.1 Event yield asymmetries . . . . 34
4.2.2 Event based fit . . . . 34
4.3 Determination of $\Sigma_{\eta'}$ . . . . 34
4.3.1 Application of event based fit to toy Monte Carlo data . . . . 34
4.3.2 Application of event based fit to data . . . . 34

**6 Summary and outlook** **27**

**A Useful information** **21**

**Bibliography** **23**

**List of Figures** **25**

**List of Tables** **27**

CHAPTER 4

# Extraction of the beam asymmetries $\Sigma_\eta$ and $\Sigma_{\eta'}$

The beam asymmetry $\Sigma$ is observable when a linearly polarized photon beam and unpolarized liquid hydrogen target are employed. The polarized cross section $\frac{d\sigma}{d\Omega}_{\text{pol}}$ is not symmetric in the azimuthal angle $\phi$ anymore as opposed to the unpolarized cross section $\frac{d\sigma}{d\Omega}_0$. It is rather modulated by a cosine dependence which scales with the polarization observable $\Sigma$ and the (linear) beam polarization $p_\gamma$, see equation (4.1) [San+11].

$$\frac{d\sigma}{d\Omega}_{\text{pol}} = \frac{d\sigma}{d\Omega}_0 \cdot \left[1 - p_\gamma \Sigma \cos(2\varphi)\right] \tag{4.1}$$

Since the incident photon beam is polarized, photon momentum $\vec{k}$ and polarization $\vec{\epsilon}$ span a plane which is referred to as the beam polarization plane. This plane is tilted by the angle $\varphi$ with respect to the reaction plane which is defined by the final state momenta. Naturally, this plane builds the angle $\phi$ in the laboratory system. At the same time the angle of the beam polarization plane in the same reference frame is defined as $\alpha$. It holds

$$\varphi = \alpha - \phi. \tag{4.2}$$

Figure 4.1 illustrates definitions of all angles and planes. Theoretically the beam asymmetry can be

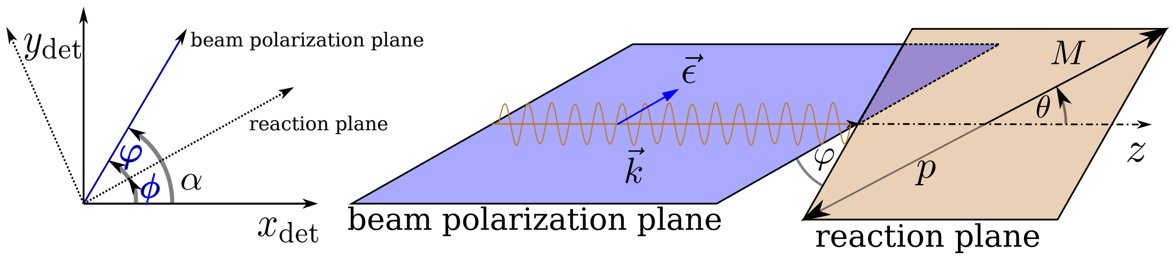


**Figure 4.1:** Left: Definition of angles $\alpha, \phi, \varphi$. Right: Photon momentum $\vec{k}$ and polarization $\vec{\epsilon}$ define the beam polarization plane while the reaction plane is defined by the recoil proton $p$ and produced meson $M$.

determined by a measurement of the cross section and a fit using equation (4.1). However, when calculating polarized cross sections, it is important to have good control over flux normalization and detector acceptance in three dimensions ($E_\gamma, \cos\theta, \phi$). To avoid this, the measurement of asymmetries can be used to access the polarization observable $\Sigma$ instead. Particularly, data is taken for two distinct orthogonal polarization settings corresponding to $\alpha = \pm 45°$.

This chapter will illustrate the process of determining the beam asymmetry for $\eta$ and $\eta'$ photoproduction. The published results of $\Sigma_\eta$ [Afz19; Afz+20] are used to check the accuracy and functionality of employed bayesian methods. Bayesian methods, as well as traditional frequentist approaches are used afterwards to extract new results for $\Sigma_{\eta'}$. First, the used methods will be presented and subsequently their application for each final state, respectively.

## 4.1 Methods

methods

### 4.1.1 Event yield asymmetries

**Frequentist**

**Bayesian**

### 4.1.2 Event based fit

**Frequentist**

**Bayesian**

## 4.2 Determination of $\Sigma_\eta$ using Bayesian statistics

### 4.2.1 Event yield asymmetries

**Application of method to toy Monte Carlo data**

**Application of method to data**

### 4.2.2 Event based fit

**Application of method to toy Monte Carlo data**

**Application of method to data**

## 4.3 Determination of $\Sigma_{\eta'}$

### 4.3.1 Application of event based fit to toy Monte Carlo data

### 4.3.2 Application of event based fit to data

# Bibliography

[San+11] A. M. Sandorfi, S. Hoblit, H. Kamano and T.-S. H. Lee,
*Determining pseudoscalar meson photoproduction amplitudes from complete experiments*,
Journal of Physics G: Nuclear and Particle Physics **38** (2011) 053001, ISSN: 1361-6471,
URL: `http://dx.doi.org/10.1088/0954-3899/38/5/053001`.

[Afz19] F. N. Afzal, *Measurement of the beam and helicity asymmetries in the reactions $\gamma p \to p\pi^0$ and $\gamma p \to p\eta$*,
PhD thesis: Rheinische Friedrich-Wilhelms-Universität Bonn, 2019,
URL: `https://hdl.handle.net/20.500.11811/8064` (cit. on p. 34).

[Afz+20] F. Afzal et al.,
*Observation of the $p\eta'$ Cusp in the New Precise Beam Asymmetry $\Sigma$ Data for $\gamma p \to p\eta$*,
Phys. Rev. Lett. **125** (15 2020) 152002,
URL: `https://link.aps.org/doi/10.1103/PhysRevLett.125.152002`.

# List of Figures


1.1 Running coupling of QCD. The colored data points represent different methods to obtain a value for $\alpha_s$. For more details it may be referred to [**pdg**]. . . . . . . . . . . 2

1.2 Calculated nucleon (isospin $I = 1/2$) resonances compared to measurements. Left in each column are the calculations [**bonnmodel**], the middle shows the measurements and PDG rating [**pdg**] . . . . . . . . . . . . . . . . . . . . . . . . . . . . . . . 3

1.3 Feynman diagram for the s-channel photoproduction of pseudoscalar mesons, adapted from [Afz19] . . . . . . . . . . . . . . . . . . . . . . . . . . . . . . . . . . 4

2.1 [**cb**] . . . . . . . . . . . . . . . . . . . . . . . . . . . . . . . . . . . . . . 7

2.2 [**cb**] . . . . . . . . . . . . . . . . . . . . . . . . . . . . . . . . . . . . . . 8

2.3 [**cb**] . . . . . . . . . . . . . . . . . . . . . . . . . . . . . . . . . . . . . . 8

2.4 D. Walther in [**urban**] . . . . . . . . . . . . . . . . . . . . . . . . . . . . . 9

2.5 [**cb**] . . . . . . . . . . . . . . . . . . . . . . . . . . . . . . . . . . . . . . 9

2.6 [**cb**] . . . . . . . . . . . . . . . . . . . . . . . . . . . . . . . . . . . . . . 10

3.1 Distribution of event classes in $\eta' \rightarrow \gamma\gamma$ production . . . . . . . . . . . . . . . . . . 12

3.2 Time information of all final state particles and the beam photon for 3PED $\eta'$ production 13

3.3 Reaction time $t_r$ for 3PED $\eta'$ production . . . . . . . . . . . . . . . . . . . . . . . 14

3.4 Coplanarity of the $p\eta'$ final state with all other cuts applied for the energy bin $1\,500\,\text{MeV} \leq E_\gamma < 1\,600\,\text{MeV}$. The vertical dashed lines show the cut ranges obtained from a gaussian fit to the data (open circles). The solid black histograms represent fitted MC data of $\eta' \rightarrow \gamma\gamma$ . . . . . . . . . . . . . . . . . . . . . . . . 18

3.5 Polar angle difference of the $p\eta'$ final state with all other cuts applied for the energy bin $1\,500\,\text{MeV} \leq E_\gamma < 1\,600\,\text{MeV}$. The vertical dashed lines show the cut ranges obtained from a gaussian fit to the data (open circles). The solid black histograms represent fitted MC data of $\eta' \rightarrow \gamma\gamma$ . . . . . . . . . . . . . . . . . . . . . . . . 18

3.6 Missing mass of the $p\eta'$ final state with all other cuts applied for the energy bin $1\,500\,\text{MeV} \leq E_\gamma < 1\,600\,\text{MeV}$. The vertical dashed lines show the cut ranges obtained from a fit to data (open circles) employing a Novosibirsk function. The solid colored histograms represent fitted MC data from relevant photoproduction reactions: in black $\eta'$, in green $\pi^0$, in red $\eta$, in blue $\omega$, in yellow $2\pi^0$, magenta $\pi^0\eta$. The turquoise histogram is the sum of all MC histograms. . . . . . . . . . . . . . . . . . . . . . . . 19

3.7 Invariant mass of the $p\eta'$ final state with all other cuts applied for all energy and angular bins. The open circles represent the measured data, the solid colored histograms fitted MC data from relevant photoproduction reactions: in black $\eta'$, in green $\pi^0$, in red $\eta$, in blue $\omega$, in yellow $2\pi^0$ and in magenta $\pi^0\eta$. The turquoise histogram is the sum of all MC histograms. . . . . . . . . . 20
3.8 Invariant mass of the $p\eta'$ final state with all other cuts applied for the energy bin $1\,500\,\text{MeV} \leq E_\gamma < 1\,600\,\text{MeV}$. The vertical dashed lines show the cut ranges obtained from a gaussian fit to the $\eta'$ MC data (solid black histogram). The open circles represent the measured data, the solid colored histograms fitted MC data from relevant photoproduction reactions: in black $\eta'$, in green $\pi^0$, in red $\eta$, in blue $\omega$, in yellow $2\pi^0$ and in magenta $\pi^0\eta$. The turquoise histogram is the sum of all MC histograms. . . . . . . . . . 21
3.9 Acceptance for the reaction $\gamma p \to p\eta'$ after all cuts that have been discussed so far for 2.5PED and 3PED events . . . . . . . . . . 22
3.10 Fraction of background events in the analyzed beam energy and angular bins. . . . . 23
3.11 Acceptance for possible background contributions . . . . . . . . . . 24
3.12 Generated energies of the two lowest energy photons in $2\pi^0$ photoproduction MC data. The threshold of 20 MeV is marked by a vertical red line. Lowest energy photon is shown on the top, second lowest energy photon is shown on the bottom. . . . . . . 25
3.13 Generated energies of the two lowest energy photons in $2\pi^0$ and $\pi^0\eta$ photoproduction MC data. The threshold of 20 MeV is marked by a vertical red line. Lowest energy photon is shown on the top, second lowest energy photon is shown on the bottom. . . 26
3.14 Polar angle difference $\Delta\theta$ between the photon with second highest energy and second lowest energy of the $\pi^0\eta$ final state. . . . . . . . . . 26
3.15 Illustration of the misidentification process during reconstruction . . . . . . . . . . 27
3.16 Generated CMS angle $\cos\theta_{\text{gen.}}$ vs. reconstructed CMS angle $\cos\theta_{\text{rec.}}$ for both background reactions. The slope $\cos\theta_{\text{gen.}} = \cos\theta_{\text{rec.}}$ is indicated by the solid line. . . 28
3.17 Detector hits of the recoil proton, as obtained from MC data for the production of $\eta'$, $2\pi^0$ and $\pi^0\eta$. CB: Crystal Barrel, FW: forward dector, MT: MiniTAPS . . . . . . 30
3.18 Difference in measured and calculated beam energy. Data points are shown as open circles, MC data as solid histograms: in black $\eta'$, in green $\pi^0$, in red $\eta$, in blue $\omega$, in yellow $2\pi^0$ and in magenta $\pi^0\eta$. The turquoise histogram is the sum of all MC histograms. . . . . . . . . . 31

4.1 Left: Definition of angles $\alpha, \phi, \varphi$. Right: Photon momentum $\vec{k}$ and polarization $\vec{\epsilon}$ define the beam polarization plane while the reaction plane is defined by the recoil proton $p$ and produced meson $M$. . . . . . . . . . 33

# List of Tables


1.1 Summary of the particles of the SM . . . . . . . . . . . . . . . . . . . . . . . . . . . 1
1.2 Allowed quantum numbers for the intermediate resonance state $N^*/\Delta^*$ . . . . . . . . . 4

3.1 The five most probable decay modes of the $\eta'$ meson. The most probable further decay with according branching ratio is shown in brackets.[**pdg**] . . . . . . . . . . . . 11
3.2 Examined MC reactions that were used in sum for the fit . . . . . . . . . . . . . . . . 16
3.3 Fit functions and cut ranges for each variable . . . . . . . . . . . . . . . . . . . . . . 17
3.4 Total cross sections $\sigma$ in the energy range 1 500 to 1 800 MeV, branching ratios (BR) to $n\gamma$ final states and maximum acceptance $\tilde{A}$ for signal and possible background contributions . . . . . . . . . . . . . . . . . . . . . . . . . . . . . . . . . . . . 23
3.5 Relative loss in signal and background events if a cut on $\Delta E$ is applied. . . . . . . . . . 29